

Generalised Precoded Spatial Modulation for Integrated Wireless Information and Power Transfer

Rong Zhang, Lie-Liang Yang and Lajos Hanzo

Communications, Signal Processing and Control, School of ECS, University of Southampton, SO17 1BJ, UK

Email: rz,lly,lh@ecs.soton.ac.uk, <http://www-mobile.ecs.soton.ac.uk>

arXiv:1705.11076v1 [cs.IT] 31 May 2017

Abstract—Conventional wireless information transfer by modulating the amplitude, phase or frequency leads to an inevitable Rate-Energy (RE) trade-off in the presence of simultaneous Wireless Power Transfer (WPT). In echoing Varshney’s seminal concept of *jointly* transmitting both information and energy, we propose the so-called Generalised Precoded Spatial Modulation (GPSM) aided Integrated Wireless Information and Power Transfer (IWIPT) concept employing a power-split receiver. The principle of GPSM is that a particular subset of *Receive Antennas* (RA) is activated and the activation pattern itself conveys useful information. Hence, the novelty of our GPSM aided IWIPT concept is that RA pattern-based information transfer is used in addition to the conventional waveform-based information carried by the classic M -ary PSK/QAM modulation. Following the Radio Frequency (RF) to Direct Current (DC) power conversion invoked for WPT at the power-split receiver, the non-coherent detector simply compares the remaining received power accumulated by each legitimate RA pattern for the sake of identifying the most likely RA. This operation is then followed by down-conversion and conventional Base Band (BB) M -ary PSK/QAM detection. Both our analysis and simulations show that the RA pattern-based information transfer represented in the Spatial Domain (SD) exhibits a beneficial immunity to any potential power-conversion induced performance degradation and hence improves the overall RE trade-off when additionally the waveform-based information transfer is also taken into account. Moreover, we investigate the impact of realistic imperfect Channel State Information at the Transmitter (CSIT) as well as that of the antenna correlations encountered. Finally, the system’s asymptotic performance is characterised in the context of large-scale Multiple Input Multiple Output (MIMO) systems.

I. INTRODUCTION

1) *Motivation*: In thermal and statistical physics, the earliest and most famous thought experiment regarding information and energy was conceived by Maxwell in 1867, which is referred to as “Maxwell’s Demon” [1], where the second law of thermo-dynamics was hypothetically violated by the bold hypothesis of information to energy conversion. This stimulated further intriguing research in the mid-20th century as to whether information processing itself dissipates energy, which subsequently led to “Landauer’s principle” [2], [3] suggesting that thermo-dynamically reversible manipulations of information in computing, measurement and communications do not necessarily dissipate energy, since no energy is required to perform mathematical calculations. This principle has thus

led to further research in the area of reversible computing and reversible electronic circuits [4]. Although elusive, a so-called “information heat engine” was experimentally demonstrated in [5] for showcasing information to energy conversion with the aid of feedback control.

Despite the fact that information to energy conversion is in its infancy, it was suggested from a fundamental perspective [6] that the currently separate treatment of information and energy has to be challenged in the practical design of engineering systems. Naturally, information is carried by attaching itself to a physical medium, such as waves or particles. In molecular and nano communications, information is delivered by conveying encoded particles from the source to destination [7], [8]. Similarly, in optical communications, information is delivered by photons having information-dependent intensities, which may be detected by a photon-counting process [9], [10]. Given the nature of the process, the system is capable of providing a heating/illumination/propulsion function. Both of the above examples suggest that the underlying matter that carries information can be effectively reused for diverse applications. The explicit concept of transporting both information and energy simultaneously was raised by the authors of [11], [12], [13] in the context of power-line communications, where information is conveyed by wires that carry electricity. This topic was recently further extended to wireless communications, since it is desirable that a mobile device is free from being tethered in any way, as prophesied a century ago [14].

2) *Background*: Before delving into the topic of Simultaneous Wireless Information and Power Transfer (SWIPT), a brief historical portrayal of Wireless Power Transfer (WPT) is warranted [15]. The earliest experiments on WPT were conducted by Tesla with the ultimate goal of creating a worldwide wireless power distribution system [16]. In the mid-20th century, one of the most influential projects was the microwave-powered helicopter [17]. Similarly, the National Aeronautics and Space Administration’s (NASA) feasibility study of the space-solar program [18] attracted global attention. The need for small to moderate power requirements (upto hundreds of watts) and near-field (upto a few meters) WPT increased substantially owing to the development of electronic devices in the late 20th century. Hence the wireless power consortium was established for promoting the standardization for wireless charging, known as Qi¹. WPT can be carried out in two basic ways, namely based on either electromagnetic

The financial support of the EPSRC under the India-UK Advanced Technology Centre (IU-ATC), that of the EU under the Concerto project as well as that of the European Research Council’s (ERC) Advanced Fellow Grant is gratefully acknowledged.

¹see websites: <http://www.wirelesspowerconsortium.com/>

induction in the form of inductive coupling and resonant coupling relying on coils or with the aid of electromagnetic *radiation* using microwave frequencies by relying on so-called rectennas, which will be discussed in Section II-C. At the time of writing there are already numerous WPT applications, ranging from wirelessly charged mobile phones [19] to wirelessly powered medical implants [20] and to ‘immortal’ sensor networks [21] in addition to passive Radio-frequency IDentification (RFID) devices [22]. Furthermore, along with successful start-up companies like WiTricity and Powercast ², it is thus the maturing WPT and wireless communications fields that make the SWIPT an interesting emerging research topic.

However, the current research of SWIPT is still in its infancy and hence there is a paucity of literature, which may be classified as follows. The first set of contributions considered *one-way* SWIPT, where the transmitter simultaneously conveys both information and power to the receiver that may be operated in two different modes [23], namely either on a time-division basis or on a power-split basis. To be more specific, in the time-division mode, the receiver alternatively and opportunistically acts as an information detector and power converter [24]. On the other hand, in the power-split mode, a portion of the received power is used for powering the receiver and the remaining received power is used for retrieving information [25], [26]. The second set of contributions considered *two-way* SWIPT. Specifically, the authors of [27], [28] investigated the scenario, where the transmitter conveys power to the receiver, which is converted to Direct Current (DC) power and reused for the destination’s information transmission in the reverse direction. This mode of operation is similar to that of the passive RFID devices and hence it may be referred to as being *two-way half-duplex*. Distinctively, [29] investigated a *two-way full-duplex* operational mode, where a pair of nodes interactively communicates and exchanges power. The final set of treatises considered a range of energy-transfer-aided systems, such as multi-carrier systems [30], relay-assisted systems [31], interference-limited arrangements [32], beamforming-assisted regimes [33], [34], multiple access [35] and unicast/multicast scenarios [36].

3) *Novelty*: A close inspection of the existing literature reveals that most of the current designs are centered on the information transfer strategy in the presence of power transfer, while satisfying a specific received energy constraint. It would be however more beneficial to aim for the full “integration” of information and power transfer as the ultimate objective in the spirit of Varshney’s concept [12], who proposed that energy and information transfer should be innately inter-linked.

To be more explicit, in one-way SWIPT equipped with a power-split receiver ³, an inevitable Rate-Energy (RE) trade-off has to be obeyed, which simply suggests that the more power is transferred for powering the receiver, the lower the communications rate becomes. This observation is intuitive, since from an information theoretic point of view, less power is left for information transfer, which inevitably leads to a

reduced information rate. Naturally, having a reduced power for information transfer implies that the information becomes more prone to errors. One of the fundamental reasons for the RE trade-off is that information is conventionally transferred by modulating the amplitude, phase or frequency, which are naturally subjected to channel-induced distortion, noise and power-splitting. In order to eliminate these impediments, we propose a completely different modulation type for Integrated Wireless Information and Power Transfer (IWIPT), where information is carried not by *waveforms* but by *patterns*.

Explicitly, a multi-antenna aided system is conceived for IWIPT, where the specific Receive Antenna (RA) patterns are used for conveying information, while simultaneously transferring power.

- We achieve this with the aid of our recently proposed Generalised Pre-coding aided Spatial Modulation (GPSM) scheme [37], where information is conveyed by appropriately selecting the RA indices for information transfer in addition to the information carried by the conventional M -ary PSK/QAM modulation ⁴.
- We show that the RA pattern-based information transfer represented in the Spatial Domain (SD) exhibits a beneficial immunity to any performance degradation imposed by the Radio Frequency (RF) to DC power conversion in a power-split receiver and that our GPSM scheme is capable of improving the overall RE trade-off, when additionally the waveform-based information transfer represented in the classic time domain is also taken into account.

4) *Organisation*: The rest of our paper is organised as follows. In Section II, we introduce the underlying concept as well as the transceiver architecture of the GPSM aided IWIPT system employing a power-split receiver. This is followed by our analytical study in Section III, where we demonstrate that the proposed RA pattern-based information transfer represented in the SD exhibits a beneficial immunity to RF to DC power conversion induced performance erosion. We then continue by characterizing the RE trade-off of the overall system. Our simulation results are provided in Section IV, while we conclude in Section V.

II. SYSTEM MODEL

Our proposed GPSM aided IWIPT system relies on the availability of Channel State Information at the Transmitter (CSIT) for supporting Transmitter Pre-Coding (TPC). This scenario has been widely considered in the SWIPT literature [23], [27], [32], [33], [34], since it is desirable to shift most/all signal processing demands from the less powerful Down-Link (DL) receiver that may be passive or semi-passive to the more powerful DL transmitter that may have access to the mains power.

A. Conceptual Description

Consider a Multiple Input Multiple Output (MIMO) system equipped with N_t Transmit Antennas (TA) and N_r RAs, where

²see websites: <http://www.witricity.com/> and <http://www.powercastco.com/>

³The time-division receiver is conceptually simple but it has been shown to be sub-optimum [12]. Hence it is not considered in this paper.

⁴Spatial Modulation [38], [39] conveys extra information by appropriately selecting the *transmit* antenna indices, but our GPSM scheme conveys extra information by appropriately selecting the *receive* antenna indices [37].

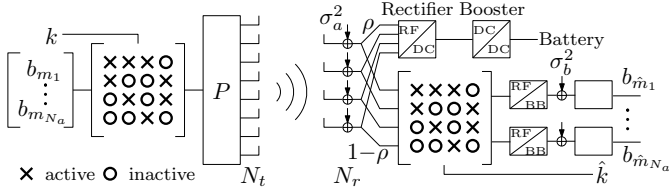


Fig. 1. Transceiver architecture of GPSM aided IWIPT. For example, activating $N_a = 2$ RAs out of $N_r = 4$ RAs results in a total of $|\mathcal{C}_t| = 6$ legitimate activation patterns, i.e. the patterns of $\mathcal{C}_t = \{[1, 2], [1, 3], [1, 4], [2, 3], [2, 4], [3, 4]\}$. This configuration delivers $k_{ant} = 2$ bits of information because $\lfloor \log_2(|\mathcal{C}_t|) \rfloor = 2$. Upon selecting for example $\mathcal{C} = \{\mathcal{C}_t(1), \mathcal{C}_t(2), \mathcal{C}_t(3), \mathcal{C}_t(4)\}$, we have the following mapping between the SD symbol and the activation patterns $k = 1 \mapsto \mathcal{C}(1) = [1, 2]$, $k = 2 \mapsto \mathcal{C}(2) = [1, 3]$, $k = 3 \mapsto \mathcal{C}(3) = [1, 4]$ and $k = 4 \mapsto \mathcal{C}(4) = [2, 3]$.

we assume $N_t \geq N_r$. In this MIMO set-up, a maximum of $N_r = \min(N_t, N_r)$ parallel data streams may be supported by conventional waveform-based information transfer, conveying a total of $k_{eff} = N_r k_{mod}$ bits altogether, where $k_{mod} = \log_2(M)$ denotes the number of bits per symbol of a conventional M -ary PSK/QAM scheme and its alphabet is denoted by \mathcal{A} . The TPC matrix of $\mathbf{P} \in \mathbb{C}^{N_t \times N_r}$ may be used for pro-actively mitigating the Inter-Channel Interference (ICI) at the transmitter by pre-processing the source signal before its transmission upon exploiting the knowledge of the CSIT. As a benefit, a low-complexity single-stream detection scheme may be used by the receiver, because the ICI is eliminated at the transmitter.

In contrast to the above-mentioned classic waveform-based multiplexing of N_r data streams, in our GPSM scheme a total of $N_a < N_r$ RAs are activated so as to facilitate the simultaneous transmission of N_a data streams, where the particular *pattern* of the N_a RAs activated conveys information in form of so-called SD symbols in addition to the information carried by the conventional M -ary PSK/QAM modulated symbols as seen in Fig 1⁵. Hence, the number of bits in GPSM conveyed by a SD symbol becomes $k_{ant} = \lfloor \log_2(|\mathcal{C}_t|) \rfloor$, where the set \mathcal{C}_t contains all the combinations associated with choosing N_a activated RAs out of N_r RAs. As a result, the total number of bits transmitted by the GPSM scheme is $k_{eff} = k_{ant} + N_a k_{mod}$. To assist our further discussions, let us define the set of selected activation patterns as $\mathcal{C} \subset \mathcal{C}_t$. We also let $\mathcal{C}(k)$ and $\mathcal{C}(k, i)$ denote the k th RA activation pattern and the i th activated RA in the k th activation pattern, respectively. Finally, it is plausible that the conventional MIMO scheme using purely waveform-based information transfer obeys $N_a = N_r$.

B. IWIPT Transmitter

More specifically, let \mathbf{s}_m^k be an *explicit* representation of a so-called super-symbol $\mathbf{s} \in \mathbb{C}^{N_r \times 1}$, indicating that the RA pattern k is activated and N_a conventional modulated symbols $\mathbf{b}_m = [b_{m_1}, \dots, b_{m_{N_a}}]^T \in \mathbb{C}^{N_a \times 1}$ are transmitted, where we have $b_{m_i} \in \mathcal{A}$ and $\mathbb{E}[|b_{m_i}|^2] = 1, \forall i \in [1, N_a]$. In other words,

⁵Note that in our GPSM scheme, it is not necessary to convey any additional information by a conventional M -ary PSK/QAM scheme, we may consider a pure spatial modulation-aided system.

we have the relationship

$$\mathbf{s}_m^k = \mathbf{\Omega}_k \mathbf{b}_m, \quad (1)$$

where $\mathbf{\Omega}_k = \mathbf{I}[:, \mathcal{C}(k)]$ is constituted by the specifically selected columns determined by $\mathcal{C}(k)$ of an identity matrix of \mathbf{I}_{N_r} . Following TPC, the resultant transmit signal $\mathbf{x} \in \mathbb{C}^{N_t \times 1}$ may be written as

$$\mathbf{x} = \sqrt{\beta_s / N_a} \mathbf{P} \mathbf{s}_m^k. \quad (2)$$

In order to avoid any power fluctuation during the pre-processing, we introduce the scaling factor of β_s designed for maintaining the power-constraint of $\|\mathbf{x}\|^2 = 1$. As a natural requirement, the TPC matrix has to ensure that no energy leaks into the RA-elements of the unintended RA patterns. Hence, the classic linear Channel Inversion (CI)-based TPC [40], [41] may be used, which is formulated as

$$\mathbf{P} = \mathbf{H}^H (\mathbf{H} \mathbf{H}^H)^{-1}, \quad (3)$$

where $\mathbf{H} \in \mathbb{C}^{N_r \times N_t}$ represents the MIMO channel involved. We assume furthermore that each entry of \mathbf{H} undergoes frequency-flat Rayleigh fading and it is uncorrelated between different super-symbol transmissions, while remains constant within the duration of a super-symbol's transmission. The power-normalisation factor of the output power after pre-processing is given by

$$\beta_s = N_a / \mathbf{s}^H (\mathbf{H} \mathbf{H}^H)^{-1} \mathbf{s}. \quad (4)$$

The Base Band (BB) signal \mathbf{x} is then up converted to \mathbf{x}^{RF} and sent through N_t TAs.

C. IWIPT Receiver

1) *Architecture*: The power-split receiver of Fig 1 is employed [23], where we have a power transfer tunnel and information transfer tunnel. As seen from Fig 1, the received signal will be first subject to power conversion at each RA using a power-splitting ratio of $\rho \in (0, 1)$ at the RF stage, where the power transfer tunnel consists of a rectifier used for converting the received RF power to DC power, which is followed by a (multi-stage) DC to DC booster. Note that from a pure WPT point of view, the RAs, the rectifier and the DC-booster are jointly known as a rectenna. After power-splitting, the remaining signal power will be used for information transfer, which relies on determining the SD symbol for RA pattern-based information transfer at the RF-stage and on detecting the conventional modulated symbols for waveform-based information transfer at the BB-stage. Note that an additional benefit of our GPSM scheme is that a reduced number of RF to BB conversion chains are required.

2) *Power Conversion*: The RF signal observed at the N_r RAs may be written as

$$\mathbf{r}^{RF} = \mathbf{H} \mathbf{x}^{RF} + \mathbf{w}_a^{RF}, \quad (5)$$

where \mathbf{w}_a^{RF} is the RF receiver's noise. The equivalent BB representation of the noise $\mathbf{w}_a \in \mathbb{C}^{N_r \times 1}$ may be modelled by a circularly symmetric complex-valued Gaussian noise vector with each entry having a zero mean and a variance of σ_a^2 , i.e. we have $\mathbb{E}[|\mathbf{w}_a|^2] = \sigma_a^2 N_r$.

At the RF-stage of Fig 1, a portion ρ of the received power is converted to DC, where the average energy transferred by the transmitter per unit time and gleaned from all the N_r RAs is represented as

$$Q = \xi \mathbb{E} \left[\rho \sum_{i=1}^{N_r} |\tilde{r}_i^{RF}|^2 \right], \quad (6)$$

where $\tilde{r}^{RF} = \mathbf{H}\mathbf{x}^{RF}$ is the noiseless part of \mathbf{r}^{RF} , representing the power transferred by the transmitter, while the additive noise of \mathbf{w}_a^{RF} in (5) is not transferred by the transmitter, it is imposed by the RF receiver. For the time being, designing adaptive RA specific power-splitting ratios $\rho_i, i \in [1, N_r]$ is set aside for our future investigations and we also set the RF to DC conversion efficiency to $\xi = 1$ in this paper.

3) *RA Pattern-based Information Transfer*: After RF to DC power conversion of each RA at a ratio of ρ , the remaining RF signal observed at the N_r RAs invoked for information transfer may be written as

$$\mathbf{y}_a^{RF} = \sqrt{1-\rho} (\mathbf{H}\mathbf{x}^{RF} + \mathbf{w}_a^{RF}), \quad (7)$$

where the SD symbol may be determined by simply sorting the remaining received power accumulated by each legitimate RA pattern, which is mathematically represented as

$$\hat{k} = \arg \max_{\ell \in [1, |\mathcal{C}|]} \left\{ \sum_{i=1}^{N_a} |y_{a, \mathcal{C}(\ell, i)}^{RF}|^2 \right\}. \quad (8)$$

Thus, correct detection is declared when we have $\hat{k} = k$. We will later show that the factor $(1-\rho)$ does not affect the detection of SD symbols and our RA pattern-based information transfer exhibits a beneficial immunity to power conversion.

4) *Waveform-based Information Transfer*: After determining the RA pattern using the non-coherent detection process of (8), we proceed with the conventional waveform-based information transfer. After RF to BB down conversion, the BB signal may be written as

$$\mathbf{y}_b = \sqrt{1-\rho} \left(\sqrt{\beta_s/N_a} \mathbf{H} \mathbf{P} \mathbf{s}_m^k + \mathbf{w}_a \right) + \mathbf{w}_b, \quad (9)$$

where $\mathbf{w}_b \in \mathbb{C}^{N_r \times 1}$ is the down-conversion induced noise, which is modelled similarly to the RF receiver's noise \mathbf{w}_a , but with a variance of σ_b^2 . We also let $\sigma_a^2 = \alpha\sigma^2$ and $\sigma_b^2 = (1-\alpha)\sigma^2$, where σ^2 represents the total noise variance at the power-split receiver of Fig 1.

Assuming that the $v_i = \mathcal{C}(k, i)$ th RA is activated, the Signal-to-Interference-plus-Noise-Ratio (SINR) γ_{v_i} of the conventional modulated symbols after power conversion is given by

$$\gamma_{v_i} = \frac{\|\mathbf{h}_{v_i} \mathbf{p}_{v_i}\|^2}{[\sigma_a^2 + \sigma_b^2/(1-\rho)]N_a/\beta_s}, \quad (10)$$

where \mathbf{h}_{v_i} is the v_i th row of \mathbf{H} representing the channel between the v_i th RA and the transmitter, while \mathbf{p}_{v_i} is the v_i th column of \mathbf{P} representing the v_i th TPC vector.

As a subsequent stage after the RA pattern determination, the detection of conventional modulated symbols is formulated

as

$$\hat{m}_i = \arg \min_{n_i \in [1, M]} \left\{ |y_{b, \hat{v}_i} - \sqrt{\frac{(1-\rho)\beta}{N_a}} \mathbf{h}_{\hat{v}_i} \mathbf{p}_{\hat{v}_i} b_{n_i}|^2 \right\}, \quad (11)$$

where $\hat{v}_i = \mathcal{C}(\hat{k}, i)$. Thus, correct detection is declared, when we have $\hat{m}_i = m_i, \forall i$.

III. SYSTEM ANALYSIS

In this section, we will first show that the RA pattern-based information transfer of (8) is immune to power conversion, since the Symbol Error Ratio (SER) of the SD symbols remains the same as in the absence of power transfer. This is then followed by our RE trade-off analysis of the overall GPSM scheme, which is constituted by both the SD symbol used for RA pattern-based information transfer and by the conventional modulated symbols employed for waveform-based information transfer.

A. Analytical SER of RA Pattern-based Information Transfer

We commence our discussion by directly stating:

Lemma III.1. *The RA pattern-based information transfer of (8) is immune to the power conversion operation of (6) for $\rho \in (0, 1)$.*

Proof: Firstly we note that (8) relies on the principle of energy detection. Hence our analysis may be performed using the equivalent BB representation of (7), as suggested in [42], which is represented as

$$\mathbf{y}_a = \sqrt{1-\rho} \left(\sqrt{\beta_s/N_a} \mathbf{H} \mathbf{P} \mathbf{s}_m^k + \mathbf{w}_a \right). \quad (12)$$

Hence (8) becomes

$$\hat{k} = \arg \max_{\ell \in [1, |\mathcal{C}|]} \left\{ \sum_{i=1}^{N_a} |y_{a, \mathcal{C}(\ell, i)}|^2 \right\}. \quad (13)$$

Given the values of N_r as well as N_a and assuming that the RA pattern $\mathcal{C}(k)$ was activated, after substituting (3) into (12), we have:

$$y_{a, v_i} = \sqrt{(1-\rho)} \left(\sqrt{\beta_s/N_a} b_{m_i} + w_{a, v_i} \right), \forall v_i \in \mathcal{C}(k), \quad (14)$$

$$y_{a, u_i} = \sqrt{(1-\rho)} w_{a, u_i}, \quad \forall u_i \in \bar{\mathcal{C}}(k), \quad (15)$$

where $\bar{\mathcal{C}}(k)$ denotes the complementary set of the activated RA pattern $\mathcal{C}(k)$ in \mathcal{C} . Furthermore, upon introducing $\sigma_{a,0}^2 = \sigma_a^2/2$, we have:

$$\begin{aligned} |y_{a, v_i}|^2 &= \mathcal{R}(y_{a, v_i})^2 + \mathcal{I}(y_{a, v_i})^2 \\ &\sim \mathcal{N} \left[\sqrt{(1-\rho)\beta_s/N_a} \mathcal{R}(b_{m_i}), (1-\rho)\sigma_{a,0}^2 \right] \\ &\quad + \mathcal{N} \left[\sqrt{(1-\rho)\beta_s/N_a} \mathcal{I}(b_{m_i}), (1-\rho)\sigma_{a,0}^2 \right], \end{aligned} \quad (16)$$

$$\begin{aligned} |y_{a, u_i}|^2 &= \mathcal{R}(w_{a, u_i})^2 + \mathcal{I}(w_{a, u_i})^2 \\ &\sim \mathcal{N} [0, (1-\rho)\sigma_{a,0}^2] + \mathcal{N} [0, (1-\rho)\sigma_{a,0}^2], \end{aligned} \quad (17)$$

where $\mathcal{R}(\cdot)$ and $\mathcal{I}(\cdot)$ represent the real and imaginary operators, respectively. As a result, by normalisation with respect to $(1 - \rho)\sigma_a^2$, we have the following observations:

$$|y_{a,v_i}|^2 \sim \chi_2^2(g; \lambda_{v_i}), \quad \forall v_i \in \mathcal{C}(k), \quad (18)$$

$$|y_{a,u_i}|^2 \sim \chi_2^2(g), \quad \forall u_i \in \bar{\mathcal{C}}(k), \quad (19)$$

where the non-centrality parameter is given by

$$\lambda_{v_i} = \beta_s |b_{m_i}|^2 / N_a \sigma_a^2. \quad (20)$$

Exploiting the fact that $\mathbb{E}[|b_{m_i}|^2] = 1, \forall i$ or $|b_{m_i}|^2 = 1, \forall i$ for PSK modulation, we have

$$\lambda = \lambda_{v_i} = \beta_s / N_a \sigma_a^2, \quad \forall v_i \quad (21)$$

Note that λ is also a random variable obeying the distribution of $f_\lambda(\lambda)$, whose analytical expression will be given in Lemma III.2.

Recall from (13) that the correct decision concerning the SD symbol occurs, when $\sum_{i=1}^{N_a} |y_{a,v_i}|^2$ is the maximum. Since the non-centrality parameter given by (20) is not a function of ρ , power conversion operation does not affect the quantity of $\sum_{i=1}^{N_a} |y_{a,v_i}|^2$. Hence, it becomes explicit that the power-splitting ratio ρ does not affect the SER e_{ant}^s of the SD symbol of our GPSM scheme for RA pattern-based information transfer expressed in Lemma III.3. ■

Lemma III.2. (Proof see Appendix C of [43]) *The distribution $f_\lambda(\lambda)$ of the non-centrality parameter λ is given by:*

$$f_\lambda(\lambda) = \frac{N_a^{N_t - N_r + 1} \sigma_a^2 / 2}{(N_t - N_r)!} e^{-\lambda N_a \sigma_a^2 / 2} (\lambda \sigma_a^2 / 2)^{N_t - N_r}. \quad (22)$$

Lemma III.3. (Proof see Theorem III.1 of [43]) *The analytical SER e_{ant}^s of the SD symbol of our GPSM scheme relying on CI TPC may be formulated as:*

$$e_{ant}^s \approx 1 - \int_0^\infty \left\{ \int_0^\infty [F_{\chi_2^2}(g)]^{N_r - N_a} f_{\chi_2^2}(g; \lambda) dg \right\}^{N_a} f_\lambda(\lambda) d\lambda, \quad (23)$$

where $F_{\chi_2^2}(g)$ represents the Cumulative Distribution Function (CDF) of a chi-square distribution having two degrees of freedom, while $f_{\chi_2^2}(g; \lambda)$ represents the Probability Distribution Function (PDF) of a non-central chi-square distribution having two degrees of freedom and non-centrality given by λ with its PDF of $f_\lambda(\lambda)$.

B. Analytical SER of Waveform-based Information Transfer

We first introduce the SER e_{mod}^s of the conventional modulated symbols $b_{m_i} \in \mathcal{A}$ for waveform-based information transfer in the *absence* of SD symbol errors. For a specific activated RA pattern in $\mathcal{C}(k)$, the SINR of (10) becomes

$$\gamma = \gamma_{v_i} = \beta_s / N_a [\sigma_a^2 + \sigma_b^2 / (1 - \rho)], \quad \forall v_i \quad (24)$$

and for the remaining deactivated RAs in $\bar{\mathcal{C}}(k)$ we have only random noise contributions of zero mean and of a variance of

$(1 - \rho)\sigma_a^2 + \sigma_b^2$. Thus the SER e_{mod}^s may be upper bounded by [44]:

$$e_{mod}^s \leq N_{min} \int_0^\infty \mathcal{Q}(d_{min} \sqrt{\gamma/2}) f_\gamma(\gamma) d\gamma, \quad (25)$$

where $f_\gamma(\gamma)$ is a scaled version of $f_\lambda(\lambda)$ given in Lemma III.2, i.e. we have $f_\gamma(\gamma) = \kappa f_\lambda(\kappa\gamma)$, where

$$\kappa = 2[\sigma_a^2 + \sigma_b^2 / (1 - \rho)] / \sigma_a^2. \quad (26)$$

Moreover, d_{min} is the minimum Euclidean distance in the conventional modulated symbol constellation, N_{min} is the average number of the nearest neighbours separated by d_{min} in the constellation and $\mathcal{Q}(\cdot)$ denotes the Gaussian \mathcal{Q} -function.

We then introduce \tilde{e}_{mod}^s for representing the SER of the conventional modulated symbols in the *presence* of SD symbol errors due to the detection of (8), which is formally given by

Lemma III.4. (Proof see Appendix A of [43]) *Given the k th activated RA pattern, the SER of the conventional modulated symbols for waveform-based information transfer in the presence of SD symbol errors can be calculated as:*

$$\tilde{e}_{mod}^s = (1 - e_{ant}^s) e_{mod}^s + \frac{e_{ant}^s}{(2^{k_{ant}} - 1)} \sum_{\ell \neq k} \underbrace{\frac{N_c e_{mod}^s + N_d e_o^s}{N_a}}_B, \quad (27)$$

where N_c and $N_d = (N_a - N_c)$ represent the number of RAs that are common and different between $\mathcal{C}(\ell)$ and $\mathcal{C}(k)$, respectively. Mathematically we have:

$$N_c = \sum_{i=1}^{N_a} \mathbb{I}[\mathcal{C}(\ell, i) \in \mathcal{C}(k)]. \quad (28)$$

Moreover, e_o^s is defined as the modulation-type-dependent SER.

Finally, when CI based TPC is introduced, only random noise may be received by the N_d RAs in $\mathcal{C}(\ell)$, thus e_o^s simply represents the SER of the conventional modulated symbols as a result of a random guess. For example, for QPSK, we have $e_o^s = 3/4$. Note that, when the SER of the SD symbols e_{ant}^s is small, we have $\tilde{e}_{mod}^s \approx e_{mod}^s$.

C. Rate Energy Trade-off

1) *DCMC Capacity Expression:* The RE trade-off may be formulated using the power conversion of (6) and comparing it directly against the Discrete-input Continuous-output Memoryless Channel (DCMC) capacity of our GPSM scheme. This is because in our GPSM scheme the SD symbols convey integer values constituted by the RA pattern index, which does not obey the shaping requirements of Gaussian signalling [45]. Hence, for simplicity's sake, we discuss the DCMC capacity of our GPSM scheme in the context of discrete-input signalling for both the SD symbol and for the conventional modulated symbols mapped to it.

The Mutual Information per Bit (MIB) $I(z; \hat{z})$ of our GPSM scheme measured between the input bits $z \in [0, 1]$ and the

corresponding demodulated output bits $\hat{z} \in [0, 1]$ is given by:

$$I(z; \hat{z}) = - \sum_z P_z \log P_z - \sum_{\hat{z}} P_{\hat{z}} \left[\sum_z P_{z|\hat{z}} \log P_{z|\hat{z}} \right] \\ = 1 + e_{eff}^b \log e_{eff}^b + (1 - e_{eff}^b) \log(1 - e_{eff}^b), \quad (29)$$

where P_z is the Probability Mass Function (PMF) of z , where we adopt the common assumption of equi-probability bits of $P_{z=0} = P_{z=1} = 1/2$. On the other hand, the conditional entropy, representing the average uncertainty about z after observing \hat{z} , is a function of the average Bit Error Ratio (BER) of our GPSM scheme, denoted as e_{eff}^b . As a result, the so-called DCMC capacity becomes

$$R = k_{eff} I(z; \hat{z}). \quad (30)$$

2) *Average BER Expression*: Let us now discuss the expression of e_{eff}^b for the sake of calculating (29) and (30), which may be derived from its accurate SER expression of both the SD symbol for the RA pattern-based information transfer given in (23) and for the conventional modulated symbols for waveform-based information transfer given in (27).

Let e_{ant}^b and \tilde{e}_{mod}^b represent the BER of the SD symbol for RA pattern-based information transfer and of the conventional modulated symbols for waveform-based information transfer. Hence, the accurate expression of the average BER of our GPSM scheme may be written as:

$$e_{eff}^b = (k_{ant} e_{ant}^b + N_a k_{mod} \tilde{e}_{mod}^b) / k_{eff} \\ = (\delta_{ant} e_{ant}^s + N_a \tilde{e}_{mod}^s) / k_{eff}, \quad (31)$$

where the second equation of (31) obeys from the relationship of

$$\tilde{e}_{mod}^b = \tilde{e}_{mod}^s / k_{mod}, \quad (32)$$

$$e_{ant}^b = \delta_{k_{ant}} e_{ant}^s / k_{ant}, \quad (33)$$

where we formulate Lemma III.5 for the expression of $\delta_{k_{ant}}$ acting as a correction factor in (31).

Lemma III.5. (Proof see Appendix B of [43]) *The generic expression of the correction factor $\delta_{k_{ant}}$ for k_{ant} bits of information is given by:*

$$\delta_{k_{ant}} = \delta_{k_{ant}-1} + \frac{2^{k_{ant}-1} - \delta_{k_{ant}-1}}{2^{k_{ant}} - 1}, \quad (34)$$

where given $\delta_0 = 0$, we can recursively determine $\delta_{k_{ant}}$.

D. Further Discussions

1) *Robustness*: The above RE trade-off is based on the assumption of having perfect CSIT. Let us now consider the system's robustness to both CSIT-errors and antenna correlations, where the expression e_{eff}^b of our GPSM scheme will be determined empirically for calculating (29) and (30).

Like in all TPC schemes, an important related aspect is its resilience to CSIT inaccuracies. In this paper, we let $\mathbf{H} = \mathbf{H}_t + \mathbf{H}_e$, where \mathbf{H}_t represents the matrix hosting the average CSI, with each entry obeying the complex Gaussian distribution of $h_t \sim \mathcal{CN}(0, \sigma_t^2)$ and \mathbf{H}_e is the instantaneous CSI error matrix obeying the complex Gaussian distribution of

$h_e \sim \mathcal{CN}(0, \sigma_e^2)$, where we have $\sigma_t^2 + \sigma_e^2 = 1$. As a result, only \mathbf{H}_t is available at the transmitter for pre-processing. There is a plethora of CSIT inaccuracy counter-measures conceived for general transmitter pre-coding schemes in the literature [46], [47], but they are beyond the scope of our discussions in this paper.

Another practical phenomenon is the presence of correlation amongst the signals at the transmit and receive antennas. The correlated MIMO channel is modelled by the widely-used Kronecker model [48], which is formulated as $\mathbf{H} = (\mathbf{R}_t^{1/2}) \mathbf{G} (\mathbf{R}_r^{1/2})^T$, with \mathbf{G} representing the original MIMO channel imposing no correlation, while \mathbf{R}_t and \mathbf{R}_r represents the correlations at the transmitter and receiver side, respectively, with the correlation entries given by $R_t(i, j) = \rho_t^{|i-j|}$ and $R_r(i, j) = \rho_r^{|i-j|}$.

2) *Asymptotic Insights*: It is also interesting to investigate the impact of power conversion on both the MIB as well as on the DCMC capacity of our GPSM scheme and to contrast it to that of the conventional CI pre-coding based MIMO scheme for large-scale MIMO settings of $N_t \rightarrow \infty$, $N_r \rightarrow \infty$ and for a fixed system load ratio of N_r/N_t .

In order to provide these asymptotic insights for these large-scale MIMO settings, we have to replace the constraint of $\|\mathbf{x}\|^2 = 1$ with its relaxed version of $\mathbb{E}[\|\mathbf{x}\|^2] = 1$. Hence instead of (4), we have the relaxed normalisation factor of

$$\beta_l = N_r / \text{Tr}[(\mathbf{H}\mathbf{H}^H)^{-1}]. \quad (35)$$

As shown in Corollary 4 of [49] and also in Chapter 14 of [50], under asymptotic settings, (35) tends to

$$\beta_l \mapsto (N_t/N_r - 1). \quad (36)$$

By exploiting (36) and by replacing (4) with (35) in the expressions of (21) and (24), we have the following deterministic quantity

$$\lambda \mapsto \lambda_d = (N_t/N_r - 1) / N_a \sigma_a^2, \quad (37)$$

$$\gamma \mapsto \gamma_d = (N_t/N_r - 1) / N_a [\sigma_a^2 + \sigma_b^2 / (1 - \rho)]. \quad (38)$$

As a result, we have

$$e_{ant,d}^s = 1 - \left\{ \int_0^\infty [F_{\chi^2_2}(g)]^{N_r - N_a} f_{\chi^2_2}(g; \lambda_d) dg \right\}^{N_a}, \quad (39)$$

$$e_{mod,d}^s = N_{min} \mathcal{Q} \left(d_{min} \sqrt{\gamma_d/2} \right). \quad (40)$$

Noting that when $e_{ant,d}^s$ is small, we arrive at the approximation $\tilde{e}_{mod,d}^s \approx e_{mod,d}^s$ as suggested by (27), thus we may obtain $e_{eff,d}^b$ by replacing e_{ant}^s and \tilde{e}_{mod}^s in (31) with their deterministic expressions in (39) and (40). Finally, by inserting $e_{eff,d}^b$ in (29) and (30) instead of e_{eff}^b , we arrive at the MIB and DCMC capacity for both our GPSM scheme as well as for the conventional CI pre-coding based MIMO scheme ($N_a = N_r$) under the asymptotic settings of $N_t \rightarrow \infty$ and $N_r \rightarrow \infty$.

IV. NUMERICAL RESULTS

Let us now consider our numerical results for characterizing the GPSM aided IWIPT for both RA pattern-based information transfer and for waveform-based information transfer relying

TABLE I

MAXIMUM ACHIEVABLE THROUGHPUT k_{eff} OF GPSM AND OF THE CONVENTIONAL MIMO CORRESPONDING TO $N_a = N_r$ (IN \bullet) UNDER SETTINGS OF $\{N_t, N_r\} = \{16, 8\}$ AND EMPLOYING QPSK MODULATION $M = 2$, WHERE $k_{eff} = k_{ant} + N_a k_{mod}$ FOR GPSM AND $k_{eff} = N_r k_{mod}$ FOR CONVENTIONAL MIMO.

N_t	N_r	N_a	M	k_{eff}
16	8	1	2	$5 = 3+1 \times 2$
16	8	2	2	$8 = 4+2 \times 2$
16	8	3	2	$11 = 5+3 \times 2$
16	8	4	2	$14 = 6+4 \times 2$
16	8	5	2	$15 = 5+5 \times 2$
16	8	6	2	$16 = 4+6 \times 2$
\bullet 16	8	8	2	$16 = 0+8 \times 2$

on the CI-based precoding of (3) under $\{N_t, N_r\} = \{16, 8\}$. Since our focus is on RA pattern-based information transfer, simple QPSK was used for the conventional data modulation component of our waveform-based information transfer. Furthermore, we investigate the scenarios correspond to $N_a = [1, \dots, 6]$ in our GPSM scheme since the setting of $N_a = 7$ results into higher complexity than the conventional CI pre-coding based MIMO bench-maker as discussed in [37]. Maximum achievable throughput under MIMO settings of $\{N_t, N_r\} = \{16, 8\}$ and employing QPSK modulation is shown in Table I, which may be used to compare our DCMC capacity related investigations. Finally, the Signal-to-Noise-Ratio (SNR) per bit is defined as $SNR_b = 1/\sigma^2(k_{eff}/N_a)$.

A. Investigation on Error Probability

Fig 2 shows the spatial SER (upper) as well as the GPSM scheme's overall BER (lower) under the power-normalisation factor of (4) for $\{N_t, N_r\} = \{16, 8\}$. Without loss of generality, we set the power-splitting ratio to $\rho = 0$ and the noise ratio to $\alpha = 1$.

Observe in the upper subplot of Fig 2 that our empirical simulation based SER results recorded for the SD symbol of the RA pattern-based information transfer accurately match the analytical results given in (23) and form tight upper bounds. Similarly, when the GPSM scheme's overall BER is considered in the lower subplot of both figures, our empirical results accurately match the analytical results given in (31).

Fig 3 shows the GPSM scheme's overall BER under the power-normalisation factor of (4) for $\{N_t, N_r\} = \{16, 8\}$, where we set the power-splitting ratio to $\rho = 0.5$ and the noise ratio to $\alpha = 0.4$. As suggested by (24), the total noise at the BB for waveform-based information transfer now becomes 1.6 times that with no WPT. Hence, we may expect to see a BER performance degradation of $10 \log_{10}(1.6) \approx 2\text{dB}$. This is clearly demonstrated in Fig 3 at BER of 10^{-5} , which implies that the RA pattern-based information transfer in our GPSM scheme is immune to the RF to DC power conversion induced performance erosion as otherwise the performance degradation would be more than 2dB.

B. Investigation on MIB

1) *Immunity to Power Conversion*: Fig 4 investigates the MIB versus energy trade-off of purely RA pattern-based information transfer for $\{N_t, N_r\} = \{16, 8\}$ and $SNR_b = 0\text{dB}$,

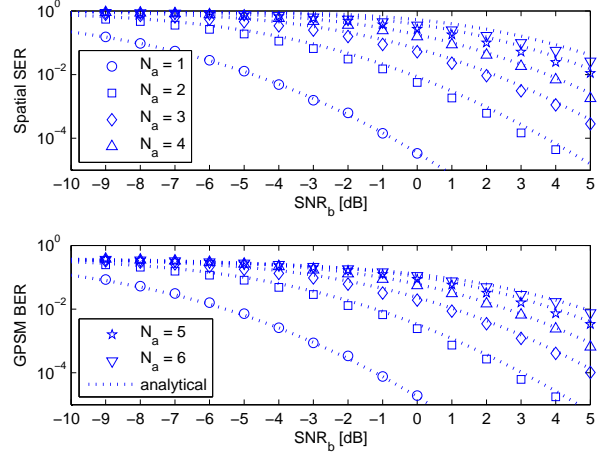


Fig. 2. Spatial SER of (23) (upper) and GPSM overall BER of (31) (lower) using CI based TPC and a power-normalisation factor of (4) under $\{N_t, N_r\} = \{16, 8\}$, where we set the power-splitting ratio to $\rho = 0$ and the noise ratio to $\alpha = 1$.

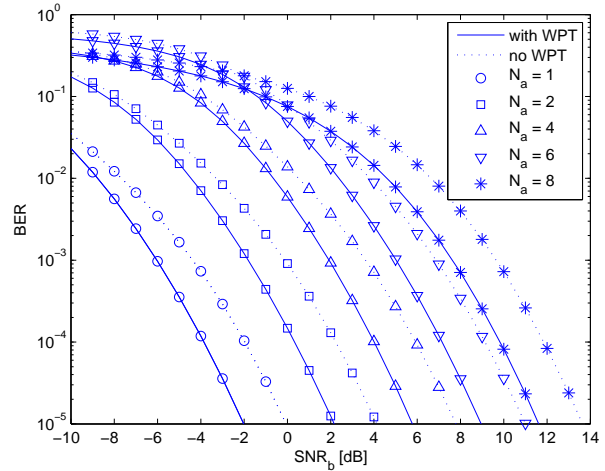


Fig. 3. BER of conventional CI pre-coding based MIMO bench-maker as well as GPSM using CI based TPC and a power-normalisation factor of (4) under $\{N_t, N_r\} = \{16, 8\}$, where we set the power-splitting ratio to $\rho = 0.5$ and the noise ratio to $\alpha = 0.4$.

where we set $\alpha = 0.4$ in the left subplot and $\alpha = 0.6$ in the right subplot. The results of MIB were evaluated from (29).

Observe from both subplots of Fig 4 that for all values of N_a , apart from setting $\rho = 1$, where the receiver acts purely as a WPT and the normalised converted energy is unity, the remaining settings of the power-splitting ratio ρ do not affect the MIB of the SD symbols in our GPSM scheme, as suggested by the horizontal lines. More explicitly, for all values of N_a seen in Fig 4, the MIB of SD symbols vs the power conversion ratio of $\rho \in [0, 0.1, \dots, 0.9]$ remains identical to that under $\rho = 0$. This implies that the RA pattern-based information transfer relying on SD symbols operates as if no WPT was provided, which justifies our Lemma III.1. Furthermore, by comparing the left and right subplot of Fig 4, it can be seen that the MIB of SD symbols becomes lower, when an increased RF receiver noise is encountered in conjunction with $\alpha = 0.6$.

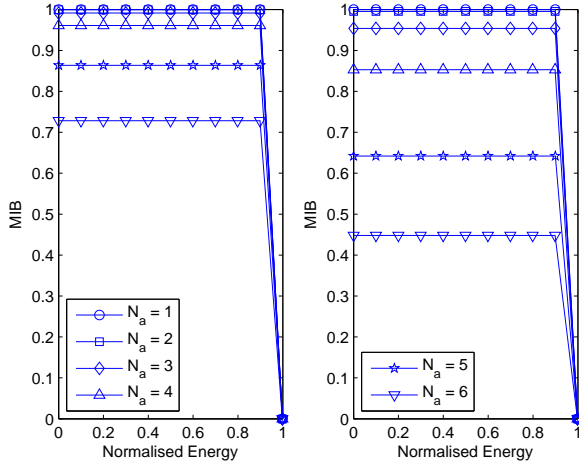


Fig. 4. MIB versus energy trade-off curve of RA pattern-based information transfer under $\{N_t, N_r\} = \{16, 8\}$ and $SNR_b = 0\text{dB}$ with $\alpha = 0.4$ (left) and $\alpha = 0.6$ (right). The MIB results were evaluated from (29).

Note that our RA pattern-based information transfer is immune to power conversion, but naturally not to the RF receiver noise.

2) *MIB versus Energy Trade-off*: Fig 5 investigates the MIB versus energy trade-off of our GPSM aided IWIPT system supporting both RA pattern-based information transfer and waveform-based information transfer for $\{N_t, N_r\} = \{16, 8\}$ and $SNR_b = 0\text{dB}$, where we set $\alpha = 0.4$ in the left subplot and $\alpha = 0.6$ in the right subplot. The results of MIB were evaluated from (29).

Observe from both subplots of Fig 5 that the near-constant MIB curves of our GPSM schemes shown in Fig 4 can no longer be maintained upon increasing the number of activated RAs, although they exhibit a less eroded MIB than the conventional CI pre-coding based MIMO scheme associated with $N_a = 8$ relying on pure waveform-based information transfer. This is because when waveform-based information transfer is also invoked, the resultant MIB of our GPSM scheme becomes more sensitive to the power conversion ratio than the purely RA pattern-based information transfer. This is evidenced in Fig 5, where the higher the value of N_a , the more conventional modulated symbols are conveyed. When comparing the left subplot to the right subplot, the MIB of our GPSM scheme appears more sensitive to the value of α . In other words, when the RF receiver's noise is more dominant ($\alpha = 0.6$), the MIB of our GPSM schemes is reduced. On the other hand, the conventional CI pre-coding based MIMO scheme is less sensitive to the value of α .

C. Investigation on DCMC Capacity

1) *DCMC Capacity versus Energy Trade-off*: Fig 6 investigates the DCMC capacity versus energy trade-off of our GPSM aided IWIPT system, where the rest of the settings were kept the same as in Fig 5. We can see that although Fig 5 suggests that the MIB of our GPSM schemes is higher than that of the conventional CI pre-coding based MIMO scheme for all power-splitting ratios for all values of N_a , when the DCMC capacity is considered in Fig 6, the GPSM curves

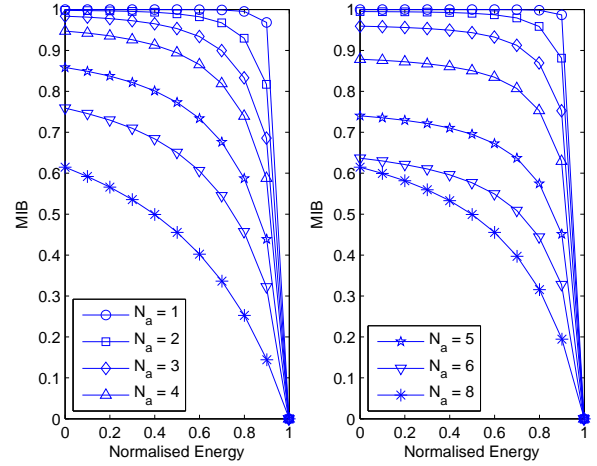


Fig. 5. MIB versus energy trade-off curve of our GPSM aided IWIPT system relying on both RA pattern-based information transfer and on waveform-based information transfer under $\{N_t, N_r\} = \{16, 8\}$ and $SNR_b = 0\text{dB}$ using $\alpha = 0.4$ (left) and $\alpha = 0.6$ (right). The MIB results were evaluated from (29).

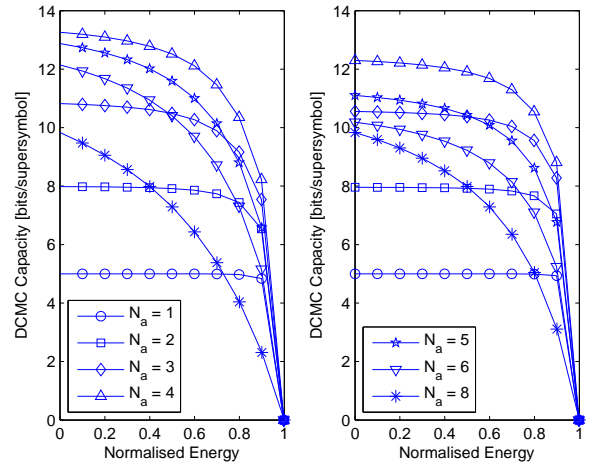


Fig. 6. DCMC capacity versus energy trade-off curve of our GPSM aided IWIPT system relying on both RA pattern-based information transfer and waveform-based information transfer under $\{N_t, N_r\} = \{16, 8\}$ and $SNR_b = 0\text{dB}$ for $\alpha = 0.4$ (left) and $\alpha = 0.6$ (right). The DCMC capacity results were evaluated from (30) and these DCMC capacity results may be compared to the maximum achievable throughput values listed in Table I.

associated with $N_a = 1$ and $N_a = 2$ exhibit intersections with the curve of the conventional CI pre-coding based MIMO scheme. By contrast, the GPSM schemes using $N_a \leq 3$ offer a DCMC capacity, which is higher than that exhibited by the conventional CI pre-coding based MIMO scheme. Finally, all of our GPSM schemes exhibit a higher degree of immunity to power conversion than the conventional CI pre-coding based MIMO scheme.

2) *DCMC Capacity versus SNR_b* : It is thus interesting to observe in detail the behaviour of our GPSM scheme associated with $N_a = 1$ and $N_a = 2$. Fig 7 compares the DCMC capacity versus SNR per bit curve of the conventional CI pre-coding based MIMO scheme relying on $N_a = 8$ to our GPSM

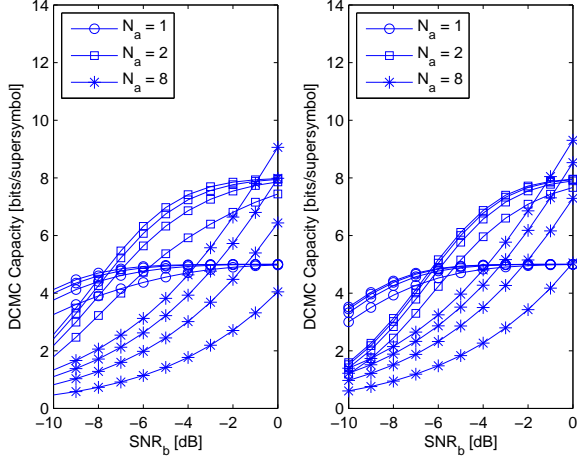


Fig. 7. DCMC capacity versus SNR per bit curve of our GPSM aided IWIPT system relying on both RA pattern-based information transfer and waveform-based information transfer under $\{N_t, N_r\} = \{16, 8\}$ with $\alpha = 0.4$ (left) and $\alpha = 0.6$ (right). For each group of curves (circle, square and no legend), the curves spanning from top to bottom correspond to $\rho = 0.2, 0.4, 0.6, 0.8$ in both plots. The DCMC capacity results were evaluated from (30) and these DCMC capacity results may be compared to the maximum achievable throughput values listed in Table I.

schemes associated with $N_a = 1$ and $N_a = 2$ supporting both RA pattern-based information transfer and waveform-based information transfer under $\{N_t, N_r\} = \{16, 8\}$ using $\alpha = 0.4$ (left) and $\alpha = 0.6$ (right). Observe for each group of curves (circle $N_a = 1$, square $N_a = 2$ and no legend $N_a = 8$) in both subplots of Fig 7 that the curves spanning from top to bottom correspond to power-splitting ratios of $\rho = 0.2, 0.4, 0.6, 0.8$.

It can also be seen in Fig 7 that our GPSM schemes using $N_a = 1$ and $N_a = 2$ offer a higher DCMC capacity than that facilitated by the conventional CI pre-coding based MIMO scheme of $N_a = 8$ in the low SNR_b range. Furthermore, observe in both subplots of Fig 7 that the DCMC capacity curves of our GPSM schemes using $N_a = 1$ and $N_a = 2$ are only slightly affected upon increasing the power-splitting ratio ρ , while we observe a dramatic difference in the DCMC capacity curves of the conventional CI pre-coding based MIMO scheme of $N_a = 8$. Thus, our GPSM schemes using $N_a = 1$ and $N_a = 2$ is significantly more immune to the performance erosion of power conversion for a wide range of SNR_b values.

D. Further Investigations

1) *Robustness Investigation:* Fig 8 investigates the DCMC capacity versus energy trade-off curves of our GPSM aided IWIPT system under $\{N_t, N_r\} = \{16, 8\}$ and $SNR_b = 0$ dB using $\alpha = 0.4$ and suffering from imperfect CSIT associated with a variance of $\sigma_e = 0.2$ (left) or when experiencing an antenna correlation associated with $\rho_t = \rho_r = 0.4$ (right). For reasons of space-economy and to avoid crowded figures, only the results of $N_a = \{2, 4, 6, 8\}$ are shown here. Observe from both subplots of Fig 8 that as expected, a DCMC capacity degradation is imposed both on our GPSM schemes and on the conventional CI pre-coding based MIMO scheme of $N_a = 8$. Nonetheless, our previous conclusions still hold, namely that

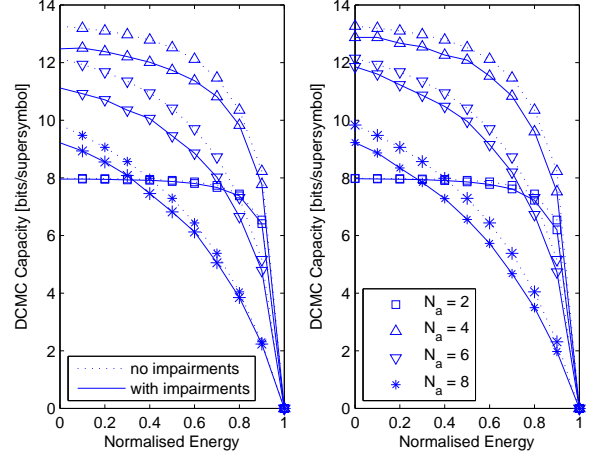


Fig. 8. DCMC capacity versus energy trade-off curve for our GPSM aided IWIPT system relying on both RA pattern-based information transfer and waveform-based information transfer under $\{N_t, N_r\} = \{16, 8\}$ and $SNR_b = 0$ dB with $\alpha = 0.4$ suffering from imperfect CSIT having a variance of $\sigma_e = 0.2$ (left) and antenna correlation associated with $\rho_t = \rho_r = 0.4$ (right). The DCMC capacity results were evaluated from (30) and these DCMC capacity results may be compared to the maximum achievable throughput values listed in Table I.

our GPSM scheme is more immune to any power conversion induced performance erosion, which is an explicit benefit of our RA pattern-based information transfer, as evidenced in Fig 8.

2) *Asymptotic Investigation:* Fig 9 characterizes the impact of power conversion both on the MIB (left) and on the DCMC capacity (right) for our GPSM scheme associated with $N_a = 1$ and $N_a = 2$ as well as for the conventional CI pre-coding based MIMO scheme using $N_a = N_r$ under asymptotic settings of $N_t = 2048$ and $N_r \in [64, 2046]$. Furthermore, $SNR_b = 0$ dB and $\alpha = 0.4$ were set in Fig 9. For each group of curves ($N_a = 1, N_a = 2$ and $N_a = N_r$) seen in both subplots of Fig 9, the curves spanning from top to bottom correspond to $\rho = 0.2, 0.4, 0.6, 0.8$.

It can be seen from the left subplot of Fig 9 that for all values of N_r/N_t , the MIB of both of our GPSM schemes is higher than that of the conventional CI pre-coding based MIMO scheme. Furthermore, the common MIB trend for all schemes is monotonically decreasing upon increasing N_r/N_t . However, we observe in the right subplot of Fig 9 that upon increasing N_r/N_t , the DCMC capacity of the conventional CI pre-coding based MIMO scheme is monotonically decreasing, while the best value of N_r/N_t may be deemed to be the one that attains the highest DCMC capacity in our GPSM schemes. Specifically, the DCMC capacity of the conventional CI pre-coding based MIMO scheme of $N_a = N_r$ is seen to be higher than that of our GPSM schemes for small values of N_r/N_t . Furthermore, our GPSM arrangement using $N_r = 2$ provides a higher DCMC capacity than the GPSM scheme relying on $N_r = 1$, when N_r/N_t is lower than about 0.5, but this trend is reversed otherwise.

Finally, a substantial DCMC capacity penalty is observed for the conventional CI pre-coding based MIMO regime of $N_a = N_r$ upon increasing the power-splitting ratio according

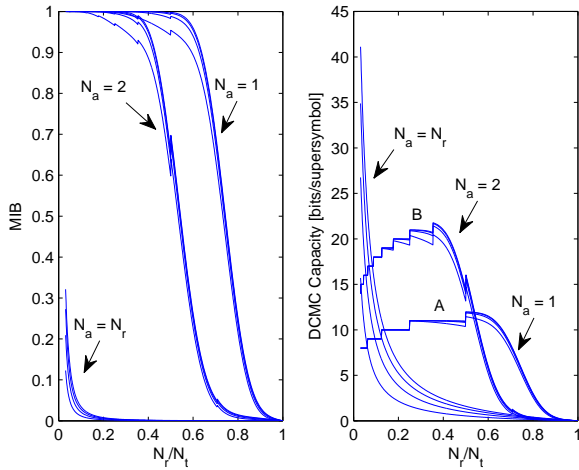


Fig. 9. The impact of power conversion on the MIB (left) and DCMC capacity (right) of both our GPSM scheme using $N_a = 1$ and $N_a = 2$ as well as the conventional CI pre-coding based MIMO scheme of $N_a = N_r$ under the asymptotic settings of $N_t = 2048$ and $N_r \in [64, 2046]$. Furthermore, we set $SNR_b = 0\text{dB}$ and $\alpha = 0.4$. For each group of curves ($N_a = 1$, $N_a = 2$ and $N_a = N_r$), the curves spanning from top to bottom correspond to $\rho = 0.2, 0.4, 0.6, 0.8$ in both subplots. The MIB and DCMC capacity results were evaluated from (29) and (30).

to $\rho = 0.2, 0.4, 0.6, 0.8$, while this trend is less obvious in both of our GPSM schemes. For example, both A and B in the right subplot of Fig 9 show that an obvious DCMC capacity penalty may only be imposed for $\rho = 0.8$. This again implies that our GPSM aided IWIPT system is less sensitive to the power conversion-induced performance erosion in the asymptotic regime.

V. CONCLUSIONS

A novel GPSM aided IWIPT system was proposed, where both RA pattern-based information transfer as well as waveform-based information transfer using conventional PSK/QAM modulation were employed. The analytical SER of the SD symbols and the BER of the overall GPSM scheme were derived. Furthermore, the MIB vs energy trade-off and the DCMC capacity vs energy trade-offs were discussed. Both the analytical and simulation results demonstrate that the RA pattern-based information transfer represented in the SD exhibits a beneficial immunity to power conversion and improves the overall RE trade-off, when the additional waveform-based QPSK information transfer is also taken into account. This conclusion holds true also both in the presence of inaccurate CSIT and of antenna correlations, even for large-scale MIMO settings. Hence, our proposed GPSM aided IWIPT system may be viewed as an instantiation of joint information and energy transfer in the spirit of Varshney's seminal concept.

VI. LIST OF PUBLICATIONS

REFERENCES

[1] K. Maruyama, F. Nori, and V. Vedral, "The physics of Maxwell's demon and information," *Reviews of Modern Physics*, vol. 81, pp. 1–23, Jan 2009.

[2] R. Landauer, "Irreversibility and heat generation in the computing process," *IBM Journal of Research and Development*, vol. 5, no. 3, pp. 183–191, 1961.

[3] —, "Dissipation and noise immunity in computation and communication," *Nature*, vol. 335, pp. 779–784, 1988.

[4] M. Saeedi and I. L. Markov, "Synthesis and optimization of reversible circuits - a survey," *ACM Computing Surveys*, vol. 45, no. 2, pp. 1–34, Mar. 2013.

[5] S. Toyabe, T. Sagawa, M. Ueda, E. Muneyuki, and M. Sano, "Experimental demonstration of information-to-energy conversion and validation of the generalized Jarzynski equality," *Nature Physics*, vol. 6, pp. 988–992, 2010.

[6] O. L. de Weck, D. Roos, and C. L. Magee, *Engineering Systems: Meeting Human Needs in a Complex Technological World*. MIT Press, 2011.

[7] T. Nakano, M. Moore, F. Wei, A. Vasilakos, and J. Shuai, "Molecular communication and networking: opportunities and challenges," *IEEE Transactions on NanoBioscience*, vol. 11, no. 2, pp. 135–148, 2012.

[8] I. F. Akyildiz, J. M. Jornet, and M. Pierobon, "Nanonetworks: a new frontier in communications," *Communications of the ACM*, vol. 54, no. 11, pp. 84–89, Nov. 2011.

[9] X. Zhou, X. Zheng, R. Zhang, and L. Hanzo, "Chip-interleaved optical code division multiple access relying on a photon-counting iterative successive interference canceller for free-space optical channels," *Optics Express*, vol. 21, no. 13, pp. 15 926–15 937, Jul 2013.

[10] L. Li, X. Zhou, R. Zhang, and L. Hanzo, "Performance and capacity analysis of poisson photon-counting based Iter-PIC OCDMA systems," *Optics Express*, vol. 21, no. 22, pp. 25 954–25 967, Nov 2013.

[11] L. Varshney, "Transporting information and energy simultaneously," in *2008 IEEE International Symposium on Information Theory*, 2008, pp. 1612–1616.

[12] —, "On energy/information cross-layer architectures," in *2012 IEEE International Symposium on Information Theory*, 2012, pp. 1356–1360.

[13] P. Grover and A. Sahai, "Shannon meets Tesla: wireless information and power transfer," in *2010 IEEE International Symposium on Information Theory*, 2010, pp. 2363–2367.

[14] N. Tesla, "The future of the wireless art," *Wireless Telegraphy & Telephony*, pp. 67–71, 1908.

[15] J. Garnica, R. Chinga, and J. Lin, "Wireless power transmission: From far-field to near-field," *Proceedings of the IEEE*, vol. 101, no. 6, pp. 1321–1331, 2013.

[16] N. Tesla, "Apparatus for transmitting electrical energy," U.S. Patent Patent 1 119 732, Dec, 1914.

[17] W. C. Brown, "The history of power transmission by radio waves," *IEEE Transactions on Microwave Theory and Techniques*, vol. 32, no. 9, pp. 1230–1242, 1984.

[18] J. McSpadden and J. Mankins, "Space solar power programs and microwave wireless power transmission technology," *IEEE Microwave Magazine*, vol. 3, no. 4, pp. 46–57, 2002.

[19] J. Lin, "Wireless power transfer for mobile applications and health effects," *IEEE Antennas and Propagation Magazine*, vol. 55, no. 2, pp. 250–253, 2013.

[20] A. Yakovlev, S. Kim, and A. Poon, "Implantable biomedical devices: wireless powering and communication," *IEEE Communications Magazine*, vol. 50, no. 4, pp. 152–159, 2012.

[21] L. Xie, Y. Shi, Y. Hou, and A. Lou, "Wireless power transfer and applications to sensor networks," *IEEE Wireless Communications*, vol. 20, no. 4, pp. 140–145, 2013.

[22] V. Chawla and D.-S. Ha, "An overview of passive RFID," *IEEE Communications Magazine*, vol. 45, no. 9, pp. 11–17, 2007.

[23] R. Zhang and C. K. Ho, "MIMO broadcasting for simultaneous wireless information and power transfer," *IEEE Transactions on Wireless Communications*, vol. 12, no. 5, pp. 1989–2001, 2013.

[24] L. Liu, R. Zhang, and K.-C. Chua, "Wireless information transfer with opportunistic energy harvesting," *IEEE Transactions on Wireless Communications*, vol. 12, no. 1, pp. 288–300, 2013.

[25] —, "Wireless information and power transfer: a dynamic power splitting approach," *IEEE Transactions on Communications*, vol. 61, no. 9, pp. 3990–4001, 2013.

[26] X. Zhou, R. Zhang, and C. K. Ho, "Wireless information and power transfer: architecture design and rate-energy tradeoff," *accepted by IEEE Transactions on Communications*.

[27] K. Huang and E. G. Larsson, "Simultaneous information-and-power transfer for broadband downlink systems," *accepted by IEEE Transactions on Signal Processing*.

- [28] H. Ju and R. Zhang, "Throughput maximization for wireless powered communication networks," *accepted by IEEE Transactions on Wireless Communications*.
- [29] P. Popovski, A. Fouladgar, and O. Simeone, "Interactive joint transfer of energy and information," *IEEE Transactions on Communications*, vol. 61, no. 5, pp. 2086–2097, 2013.
- [30] D. W. K. Ng, E. S. Lo, and R. Schober, "Wireless information and power transfer: energy efficiency optimization in OFDMA systems," *accepted by IEEE Transactions on Wireless Communications*.
- [31] I. Krikidis, S. Timotheou, and S. Sasaki, "RF energy transfer for cooperative networks: data relaying or energy harvesting?" *IEEE Communications Letters*, vol. 16, no. 11, pp. 1772–1775, 2012.
- [32] J. Park and B. Clerckx, "Joint wireless information and energy transfer in a two-user MIMO interference channel," *IEEE Transactions on Wireless Communications*, vol. 12, no. 8, pp. 4210–4221, 2013.
- [33] Z. Xiang and M. Tao, "Robust beamforming for wireless information and power transmission," *IEEE Wireless Communications Letters*, vol. 1, no. 4, pp. 372–375, 2012.
- [34] X. Chen, C. Yuen, and Z. Zhang, "Wireless energy and information transfer tradeoff for limited feedback multi-antenna systems with energy beamforming," *accepted by IEEE Transactions on Vehicular Technology*.
- [35] A. Fouladgar and O. Simeone, "On the transfer of information and energy in multi-user systems," *IEEE Communications Letters*, vol. 16, no. 11, pp. 1733–1736, 2012.
- [36] —, "Information and energy flows in graphical networks with energy transfer and reuse," *IEEE Wireless Communications Letters*, vol. 2, no. 4, pp. 371–374, 2013.
- [37] R. Zhang, L.-L. Yang, and L. Hanzo, "Generalised pre-coding aided spatial modulation," *IEEE Transactions on Wireless Communications*, vol. 12, no. 11, pp. 5434–5443, 2013.
- [38] R. Mesleh, H. Haas, S. Sinanovic, C. W. Ahn, and S. Yun, "Spatial modulation," *IEEE Transactions on Vehicular Technology*, vol. 57, no. 4, pp. 2228–2241, 2008.
- [39] M. D. Renzo, H. Haas, A. Ghayeb, S. Sugiura, and L. Hanzo, "Spatial modulation for generalized MIMO: Challenges, opportunities and implementation," *Proceedings of IEEE*. [Online]. Available: <http://eprints.soton.ac.uk/354175/>
- [40] C. Peel, B. Hochwald, and A. Swindlehurst, "A vector-perturbation technique for near-capacity multi-antenna multiuser communication—Part I: channel inversion and regularization," *IEEE Transactions on Communications*, vol. 53, no. 1, pp. 195–202, 2005.
- [41] Q. Spencer, A. Swindlehurst, and M. Haardt, "Zero-forcing methods for downlink spatial multiplexing in multiuser MIMO channels," *IEEE Transactions on Signal Processing*, vol. 52, no. 2, pp. 461–471, 2004.
- [42] H. Urick, "Energy detection of unknown deterministic signals," *Proceedings of the IEEE*, vol. 55, no. 4, pp. 523–531, 1967.
- [43] R. Zhang, L.-L. Yang, and L. Hanzo, "Error probability and capacity analysis of generalised pre-coding aided spatial modulation," *submitted to IEEE Transactions on Wireless Communications*. [Online]. Available: <http://eprints.soton.ac.uk/id/eprint/360422>
- [44] J. Proakis and M. Salehi, *Digital Communications*, 5th ed. McGraw-Hill Higher Education, 2008.
- [45] T. M. Cover and J. A. Thomas, *Elements of Information Theory*, 2nd ed. Wiley-Interscience, 2006.
- [46] D. Gesbert, "Robust linear MIMO receivers: a minimum error-rate approach," *IEEE Transactions on Signal Processing*, vol. 51, no. 11, pp. 2863–2871, 2003.
- [47] X. Zhang, D. Palomar, and B. Ottersten, "Statistically robust design of linear MIMO transceivers," *IEEE Transactions on Signal Processing*, vol. 56, no. 8, pp. 3678–3689, 2008.
- [48] J. Keromali, L. Schumacher, K. Pedersen, P. Mogensen, and F. Frederiksen, "A stochastic MIMO radio channel model with experimental validation," *IEEE Journal on Selected Areas in Communications*, vol. 20, no. 6, pp. 1211–1226, 2002.
- [49] S. Wagner, R. Couillet, M. Debbah, and D. Slock, "Large system analysis of linear precoding in correlated MISO broadcast channels under limited feedback," *IEEE Transactions on Information Theory*, vol. 58, no. 7, pp. 4509–4537, 2012.
- [50] R. Couillet and M. Debbah, *Random Matrix Methods for Wireless Communications*. New York, NY, USA: Cambridge University Press, 2011.
- [51] R. Zhang, Y. Cui, H. Claussen, H. Haas, and L. Hanzo, "Anticipatory association for indoor visible light communications: Light, follow me!" *IEEE Transactions on Wireless Communications*, submitted.
- [52] R. Zhang, M. Biagi, L. Lampe, T. D. Little, S. Mangold, and Z. Xu, "Localisation, communication and networking with VLC: Challenges and opportunities," *IEEE Journal on Selected Areas in Communications*, submitted.
- [53] R. Zhang, A. F. A. Rawi, L. D. Humphrey, and L. Hanzo, "Expanded constellation mapping for enhanced far-end-cross-talk cancellation in G.fast," *IEEE Communications Letters*, vol. 21, no. 1, pp. 56–59, Jan 2017.
- [54] R. Zhang, L. L. Yang, and L. Hanzo, "Performance analysis of non-linear generalized pre-coding aided spatial modulation," *IEEE Transactions on Wireless Communications*, vol. 15, no. 10, pp. 6731–6741, Oct 2016.
- [55] R. Zhang, H. Claussen, H. Haas, and L. Hanzo, "Energy efficient visible light communications relying on amorphous cells," *IEEE Journal on Selected Areas in Communications*, vol. 34, no. 4, pp. 894–906, April 2016.
- [56] R. Zhang, J. Wang, Z. Wang, Z. Xu, C. Zhao, and L. Hanzo, "Visible light communications in heterogeneous networks: Paving the way for user-centric design," *IEEE Wireless Communications*, vol. 22, no. 2, pp. 8–16, April 2015.
- [57] R. Zhang, L. L. Yang, and L. Hanzo, "Energy pattern aided simultaneous wireless information and power transfer," *IEEE Journal on Selected Areas in Communications*, vol. 33, no. 8, pp. 1492–1504, Aug 2015.
- [58] R. Zhang, R. G. Maunder, and L. Hanzo, "Wireless information and power transfer: from scientific hypothesis to engineering practice," *IEEE Communications Magazine*, vol. 53, no. 8, pp. 99–105, August 2015.
- [59] R. Zhang, L. L. Yang, and L. Hanzo, "Error probability and capacity analysis of generalised pre-coding aided spatial modulation," *IEEE Transactions on Wireless Communications*, vol. 14, no. 1, pp. 364–375, Jan 2015.
- [60] R. Zhang and L. Hanzo, "Multi-layer modulation for intensity-modulated direct-detection optical OFDM," *IEEE/OSA Journal of Optical Communications and Networking*, vol. 5, no. 12, pp. 1402–1412, Dec 2013.
- [61] —, "Advances in base- and mobile-station aided cooperative wireless communications: An overview," *IEEE Vehicular Technology Magazine*, vol. 8, no. 1, pp. 57–69, March 2013.
- [62] —, "Cooperative downlink multicell preprocessing relying on reduced-rate back-haul data exchange," *IEEE Transactions on Vehicular Technology*, vol. 60, no. 2, pp. 539–545, 2011.
- [63] —, "Multiple-source cooperation: From code-division multiplexing to variable-rate network coding," *IEEE Transactions on Vehicular Technology*, vol. 60, no. 3, pp. 1005–1015, March 2011.
- [64] —, "A unified treatment of superposition coding aided communications: Theory and practice," *IEEE Communications Surveys Tutorials*, vol. 13, no. 3, pp. 503–520, Third 2011.
- [65] —, "Superposition-aided delay-constrained hybrid automatic repeat request," *IEEE Transactions on Vehicular Technology*, vol. 59, no. 4, pp. 2109–2115, May 2010.
- [66] —, "Wireless cellular networks," *IEEE Vehicular Technology Magazine*, vol. 5, no. 4, pp. 31–39, 2010.
- [67] R. Zhang, L. Xu, S. Chen, and L. Hanzo, "EXIT-chart-aided hybrid multiuser detector for multicarrier interleave-division multiple access," *IEEE Transactions on Vehicular Technology*, vol. 59, no. 3, pp. 1563–1567, March 2010.
- [68] R. Zhang and L. Hanzo, "Interleaved random space time coding for multisource cooperation," *IEEE Transactions on Vehicular Technology*, vol. 58, no. 4, pp. 2120–2125, May 2009.
- [69] —, "Superposition-coding-aided multiplexed hybrid ARQ scheme for improved end-to-end transmission efficiency," *IEEE Transactions on Vehicular Technology*, vol. 58, no. 8, pp. 4681–4686, Oct 2009.
- [70] —, "Coding schemes for energy efficient multi-source cooperation aided uplink transmission," *IEEE Signal Processing Letters*, vol. 16, no. 5, pp. 438–441, May 2009.
- [71] —, "Iterative multiuser detection and channel decoding for DS-CDMA using harmony search," *IEEE Signal Processing Letters*, vol. 16, no. 10, pp. 917–920, Oct 2009.
- [72] —, "Three design aspects of multicarrier interleave division multiple access," *IEEE Transactions on Vehicular Technology*, vol. 57, no. 6, pp. 3607–3617, Nov 2008.
- [73] —, "Space-time coding for high-throughput interleave division multiplexing aided multi-source co-operation," *Electronics Letters*, vol. 44, no. 5, pp. 367–368, Feb 2008.
- [74] J. Zhang, R. Zhang, R. G. Maunder, S. Chen, and L. Hanzo, "Adaptive coding and modulation for large-scale antenna array based aeronautical

- communications in the presence of co-channel interference," *IEEE Transactions on Wireless Communications*, submitted.
- [75] Q. Wang, R. Zhang, L. L. Yang, and L. Hanzo, "Non-orthogonal multiple access: A unified perspective," *IEEE Wireless Communications*, submitted.
- [76] S. Gupta, R. Zhang, and L. Hanzo, "Energy harvesting aided device-to-device communication in the heterogeneous two-tier downlink," *IEEE Transactions on Communications*, submitted.
- [77] Y. Wang, Y. Xu, Y. Yang, X. Gao, B. Zhu, W. Cai, J. Yuan, R. Zhang, and H. Zhu, "Simultaneous light emission and detection of InGaN/GaN multiple quantum well diodes for in-plane visible light communication," *Optics Communications*, (early access), 2016.
- [78] X. Li, Y. Huo, R. Zhang, and L. Hanzo, "User-centric visible light communications for energy-efficient scalable video streaming," *IEEE Transactions on Green Communications and Networking*, vol. 1, no. 1, pp. 59–73, March 2017.
- [79] S. Gupta, R. Zhang, and L. Hanzo, "Energy harvesting aided device-to-device communication underlying the cellular downlink," *IEEE Access*, (early access), 2016.
- [80] F. Jin, X. Li, R. Zhang, C. Dong, and L. Hanzo, "Resource allocation under delay-guarantee constraints for visible-light communication," *IEEE Access*, vol. 4, pp. 7301–7312, 2016.
- [81] J. Wang, Y. Xu, X. Ling, R. Zhang, Z. Ding, and C. Zhao, "PAPR analysis for OFDM visible light communication," *Optics Express*, vol. 24, no. 24, pp. 27 457–27 474, Nov 2016.
- [82] B. Li, R. Zhang, W. Xu, C. Zhao, and L. Hanzo, "Joint dimming control and transceiver design for MIMO-aided visible light communication," *IEEE Communications Letters*, vol. 20, no. 11, pp. 2193–2196, Nov 2016.
- [83] S. Gupta, S. Kumar, R. Zhang, S. Kalyani, K. Giridhar, and L. Hanzo, "Resource allocation for D2D links in the FFR and SFR aided cellular downlink," *IEEE Transactions on Communications*, vol. 64, no. 10, pp. 4434–4448, Oct 2016.
- [84] S. Gupta, R. Zhang, and L. Hanzo, "Throughput maximization for a buffer-aided successive relaying network employing energy harvesting," *IEEE Transactions on Vehicular Technology*, vol. 65, no. 8, pp. 6758–6765, Aug 2016.
- [85] J. Jiang, P. Zhang, R. Zhang, S. Chen, and L. Hanzo, "Aperture selection for ACO-OFDM in free-space optical turbulence channel," *IEEE Transactions on Vehicular Technology*, vol. 65, no. 8, pp. 6089–6100, Aug 2016.
- [86] S. Feng, X. Li, R. Zhang, M. Jiang, and L. Hanzo, "Hybrid positioning aided amorphous-cell assisted user-centric visible light downlink techniques," *IEEE Access*, vol. 4, pp. 2705–2713, 2016.
- [87] C. Zhu, Y. Huo, J. Jiang, H. Sun, C. Dong, R. Zhang, and L. Hanzo, "Hierarchical colour-shift-keying aided layered video streaming for the visible light downlink," *IEEE Access*, vol. 4, pp. 3127–3152, 2016.
- [88] C. Zhu, Y. Huo, B. Zhang, R. Zhang, M. El-Hajjar, and L. Hanzo, "Adaptive-truncated-HARQ-aided layered video streaming relying on interlayer fec coding," *IEEE Transactions on Vehicular Technology*, vol. 65, no. 3, pp. 1506–1521, March 2016.
- [89] X. Li, F. Jin, R. Zhang, J. Wang, Z. Xu, and L. Hanzo, "Users first: User-centric cluster formation for interference-mitigation in visible-light networks," *IEEE Transactions on Wireless Communications*, vol. 15, no. 1, pp. 39–53, Jan 2016.
- [90] X. Li, R. Zhang, and L. Hanzo, "Cooperative load balancing in hybrid visible light communications and WiFi," *IEEE Transactions on Communications*, vol. 63, no. 4, pp. 1319–1329, April 2015.
- [91] F. Jin, R. Zhang, and L. Hanzo, "Resource allocation under delay-guarantee constraints for heterogeneous visible-light and RF femtocell," *IEEE Transactions on Wireless Communications*, vol. 14, no. 2, pp. 1020–1034, Feb 2015.
- [92] B. Li, J. Wang, R. Zhang, H. Shen, C. Zhao, and L. Hanzo, "Multiuser MISO transceiver design for indoor downlink visible light communication under per-LED optical power constraints," *IEEE Photonics Journal*, vol. 7, no. 4, pp. 1–15, Aug 2015.
- [93] J. Jiang, R. Zhang, and L. Hanzo, "Analysis and design of three-stage concatenated color-shift keying," *IEEE Transactions on Vehicular Technology*, vol. 64, no. 11, pp. 5126–5136, Nov 2015.
- [94] F. Wu, R. Zhang, L. L. Yang, and W. Wang, "Transmitter precoding-aided spatial modulation for secrecy communications," *IEEE Transactions on Vehicular Technology*, vol. 65, no. 1, pp. 467–471, Jan 2016.
- [95] J. Feng, R. Zhang, L. Hanzo, and S. X. Ng, "Cooperative medium access control based on spectrum leasing," *IEEE Transactions on Vehicular Technology*, vol. 63, no. 1, pp. 297–307, Jan 2014.
- [96] J. Zhang, F. Jin, R. Zhang, G. Li, and L. Hanzo, "Analysis and design of distributed antenna-aided twin-layer femto- and macrocell networks relying on fractional frequency reuse," *IEEE Transactions on Vehicular Technology*, vol. 63, no. 2, pp. 763–774, Feb 2014.
- [97] F. Jin, R. Zhang, and L. Hanzo, "Fractional frequency reuse aided twin-layer femtocell networks: Analysis, design and optimization," *IEEE Transactions on Communications*, vol. 61, no. 5, pp. 2074–2085, May 2013.
- [98] J. Zhang, R. Zhang, G. Li, and L. Hanzo, "Distributed antenna systems in fractional-frequency-reuse-aided cellular networks," *IEEE Transactions on Vehicular Technology*, vol. 62, no. 3, pp. 1340–1349, March 2013.
- [99] L. Li, X. Zhou, R. Zhang, D. Zhang, and L. Hanzo, "Performance and capacity analysis of poisson photon-counting based iter-PIC OCDMA systems," *Optics Express*, vol. 21, no. 22, pp. 25 954–25 967, Nov 2013.
- [100] X. Zhou, X. Zheng, R. Zhang, and L. Hanzo, "Chip-interleaved optical code division multiple access relying on a photon-counting iterative successive interference canceller for free-space optical channels," *Optics Express*, vol. 21, no. 13, pp. 15 926–15 937, Jul 2013.
- [101] X. Zhou, D. Zhang, R. Zhang, and L. Hanzo, "A photon-counting spatial-diversity-and-multiplexing MIMO scheme for poisson atmospheric channels relying on Q-ary PPM," *Optics Express*, vol. 20, no. 24, pp. 26 379–26 393, Nov 2012.
- [102] J. Zhang, R. Zhang, G. Li, and L. Hanzo, "Remote coalition network elements for base station cooperation aided multicell processing," *IEEE Transactions on Vehicular Technology*, vol. 61, no. 3, pp. 1406–1415, March 2012.
- [103] J. Feng, R. Zhang, and L. Hanzo, "A spectrum leasing cooperative medium access protocol and its stability analysis," *IEEE Transactions on Vehicular Technology*, vol. 61, no. 8, pp. 3718–3730, Oct 2012.
- [104] X. Xu, R. Zhang, S. Ghafoor, and L. Hanzo, "Imperfect digital-fiber-optic-link-based cooperative distributed antennas with fractional frequency reuse in multicell multiuser networks," *IEEE Transactions on Vehicular Technology*, vol. 60, no. 9, pp. 4439–4449, Nov 2011.
- [105] N. Bonello, R. Zhang, S. Chen, and L. Hanzo, "Channel code-division multiple access and its multilevel-structured LDPC-based instantiation," *IEEE Transactions on Vehicular Technology*, vol. 58, no. 5, pp. 2549–2553, Jun 2009.
- [106] —, "Reconfigurable rateless codes," *IEEE Transactions on Wireless Communications*, vol. 8, no. 11, pp. 5592–5600, November 2009.
- [107] X. Li, F. Jin, R. Zhang, and L. Hanzo, "Joint cluster formation and user association under delay guarantees in visible-light networks," in *2016 IEEE Global Telecommunications Conference*, Dec (early access) 2016.
- [108] X. Li, R. Zhang, J. Wang, and L. Hanzo, "Cell-centric and user-centric multi-user scheduling in visible light communication aided networks," in *2015 IEEE International Conference on Communications*, June 2015, pp. 5120–5125.
- [109] J. Zhang, R. Zhang, G. Li, and L. Hanzo, "Coalition network elements for base station cooperation," in *2012 IEEE Vehicular Technology Conference Fall*, Sept 2012, pp. 1–5.
- [110] F. Jin, R. Zhang, and L. Hanzo, "Frequency-swapping aided femtocells in twin-layer cellular networks relying on fractional frequency reuse," in *2012 IEEE Wireless Communications and Networking Conference*, April 2012, pp. 3097–3101.
- [111] J. Zhang, R. Zhang, X. Xu, G. Li, and L. Hanzo, "Effects of practical impairments on cooperative distributed antennas combined with fractional frequency reuse," in *2012 IEEE Wireless Communications and Networking Conference*, April 2012, pp. 1088–1092.
- [112] X. Xu, R. Zhang, and L. Hanzo, "Digital RoF aided cooperative distributed antennas with FFR in multicell multiuser networks," in *2011 IEEE Vehicular Technology Conference Fall*, Sept 2011, pp. 1–5.
- [113] J. Feng, R. Zhang, and L. Hanzo, "Auction-style cooperative medium access control," in *2011 IEEE Vehicular Technology Conference Fall*, Sept 2011, pp. 1–5.
- [114] J. Feng, R. Zhang, S. X. Ng, and L. Hanzo, "Relay selection for energy-efficient cooperative media access control," in *2011 IEEE Wireless Communications and Networking Conference*, March 2011, pp. 287–292.
- [115] R. Zhang and L. Hanzo, "Variable-rate network coding for multi-source cooperation," in *2011 IEEE Wireless Communications and Networking Conference*, March 2011, pp. 1517–1522.
- [116] R. Zhang, K. Giridhar, and L. Hanzo, "Distributed downlink multi-cell processing requiring reduced-rate back-haul data exchange," in *2011 IEEE Wireless Communications and Networking Conference*, March 2011, pp. 1277–1281.
- [117] R. Zhang, X. Xu, and L. Hanzo, "Co-channel interference mitigation capability of fixed relays connected by optical fibre," in *2010 IEEE Vehicular Technology Conference Fall*, Sept 2010, pp. 1–5.

- [118] X. Xu, R. Zhang, and L. Hanzo, "Imperfect radio over fibre aided distributed antennas with fractional frequency reuse," in *2010 IEEE Vehicular Technology Conference Fall*, Sept 2010, pp. 1–5.
- [119] R. Zhang and L. Hanzo, "Joint and distributed linear precoding for centralised and decentralised multicell processing," in *2010 IEEE Vehicular Technology Conference Fall*, Sept 2010, pp. 1–5.
- [120] —, "Harmony search aided iterative channel estimation, multiuser detection and channel decoding for DS-CDMA," in *2010 IEEE Vehicular Technology Conference Fall*, Sept 2010, pp. 1–5.
- [121] —, "Multiplexed hybrid ARQ for energy efficient transmissions under delay constraints," in *2010 IEEE International Conference on Communications*, May 2010, pp. 1–5.
- [122] M. F. U. Butt, R. Zhang, S. X. Ng, and L. Hanzo, "Superposition coding aided bi-directional relay transmission employing iteratively decoded self-concatenated convolutional codes," in *2010 IEEE Vehicular Technology Conference Spring*, May 2010, pp. 1–5.
- [123] R. Zhang and L. Hanzo, "Superposition-coding aided multiplexed hybrid ARQ scheme for improved link-layer transmission efficiency," in *2009 IEEE International Conference on Communications*, June 2009, pp. 1–5.
- [124] N. Bonello, R. Zhang, S. Chen, and L. Hanzo, "Reconfigurable rateless codes," in *2009 IEEE Vehicular Technology Conference Spring*, April 2009, pp. 1–5.
- [125] R. Zhang and L. Hanzo, "Physical-layer algebraic network coding and superposition coding for the multi-source cooperation aided uplink," in *2009 IEEE Vehicular Technology Conference Spring*, April 2009, pp. 1–5.
- [126] —, "High-throughput non-orthogonal interleaved random space-time coding for multi-source cooperation," in *2008 IEEE Global Telecommunications Conference*, Nov 2008, pp. 1–5.
- [127] N. Bonello, R. Zhang, S. Chen, and L. Hanzo, "Channel code division multiple access and its multilevel structured LDPC based instantiation," in *2008 IEEE Vehicular Technology Conference Fall*, Sept 2008, pp. 1–5.
- [128] R. Zhang, L. Xu, S. Chen, and L. Hanzo, "Repeat accumulate code division multiple access and its hybrid detection," in *2008 IEEE International Conference on Communications*, May 2008, pp. 4790–4794.
- [129] L. Xu, R. Zhang, S. Chen, and L. Hanzo, "EXIT-chart aided hybrid multiuser detector design for frequency-domain-spread chip-interleaved MC-CDMA," in *2008 IEEE Vehicular Technology Conference Spring*, May 2008, pp. 1816–1820.
- [130] R. Zhang and L. Hanzo, "Interleave division multiplexing aided space-time coding for high-throughput uplink cooperative communications," in *2008 IEEE Wireless Communications and Networking Conference*, March 2008, pp. 465–469.
- [131] —, "EXIT chart based joint code-rate and spreading-factor optimisation of single-carrier interleave division multiple access," in *2007 IEEE Wireless Communications and Networking Conference*, March 2007, pp. 735–739.